American Society of
Agricultural and Biological Engineers

An ASABE Meeting Presentation

Paper Number: 061172

Fusion of Optical and InSAR DEMs: Improving the Quality of Free Data.

Manoj Karkee

Agricultural and Biosystems Engineering, Iowa State University, karkee@iastate.edu.

Michiro Kusanagi

Remote Sensing and GIS, Asian Institute of Technology, Thailand, kusanagi@ait.ac.th.

Brian L. Steward

Agricultural and Biosystems Engineering, Iowa State University, bsteward@iastate.edu.

Written for presentation at the
2006 ASABE Annual International Meeting
Sponsored by ASABE
Portland Convention Center
Portland, Oregon
9 - 12 July 2006

Abstract. *An approach to DEM fusion was developed to improve the overall accuracy of DEMs and applied to two public products: Shuttle Radar Topographic Mission (SRTM) DEM and Advanced Spaceborne Thermal Emission and Reflection (ASTER) DEM. The relative ASTER DEM was co-registered to the SRTM coordinates and converted to the near absolute DEM by shifting the histogram to the average elevation of the SRTM DEM. The voids in one DEM were then filled through interpolation using the slope and aspect from the other DEM and using the elevation of surrounding pixels. Finally, the higher frequency components of the Optical DEM and the lower frequency components of the InSAR DEMs were filtered out, as they are more erroneous respectively. The filtered DEMs were then combined to generate the fused DEM. This approach was tested in a 6000 ha test site with fairly complex topography located in the central region of Nepal. The fused DEM shows up to 45% improvement in the accuracy measures like standard deviation and range of the errors. The approach showed promise to improve DEM accuracy and completeness while maintaining the resolution to the best of the participating DEMs. This approach increases the reliability and applicability of free and commercial DEMs produced by Optical and SAR remote sensing technologies.*

Keywords. DEMs, Stereoscopy, Interferometric SAR, Data Fusion, Spatial Frequency

Introduction

Spaceborne remote sensing has been used widely over the past few decades to generate digital elevation models (DEMs) of the land surface. Though Interferometric Synthetic Aperture Radar (InSAR) is a relatively new technology (started mainly with European Remote-Sensing Satellite (ERS-1), launched in 1991), both Optical-Stereoscopy and InSAR techniques are currently used in the field of geo-informatics. These two satellite techniques have been applied independent of each other, although several synergies can be identified to overcome the limitations of each technique.

InSAR and Optical Stereoscopy use entirely different sensing technologies. Optical stereoscopy is based on image parallax in which the coordinate difference between conjugate points in two partially overlapping images is found and based on the imaging geometry, the height information is extracted. The InSAR technique computes the height from the phase difference of the point backscatter received by either the same antenna in two passes or by the two different antennas of the same mission separated by some distance (Zebker et al., 1986; LaPrade, 1980; and Toutin, 1995).

Due to the inherent difficulties in acquiring satellite data both with the optical and the RADAR technology, they are not complete in themselves. Image matching in the stereoscopic technique may fail if the stereo images contain cloud cover, radiometric variation and low-texture. Similarly the InSAR technique may fail to estimate elevations if the RADAR images contain layovers, and shadows or suffer from temporal decorrelation (Zebker et al. 1992), and changes in atmospheric conditions between two acquisitions (Zebker et al. 1997). Due to these inherent problems, DEMs generated from either of these techniques may contain holes, poorly interpolated data and erroneous values.

Shuttle Radar Topographic Mission (SRTM) and Advanced Spaceborne Thermal Emission and Reflection (ASTER) from Earth Observing System (EOS) of National Aeronautics and Space Administration (NASA) are providing two different types of near global DEMs, the former an optical product and the later a SAR product. Both are available without cost for both commercial and non-commercial use. However, the spatial resolution of SRTM products is only 3 arcseconds or 90 m (30 m for US territories), which may not be sufficient in many engineering applications. On the other hand, EOS provides only the relative DEMs if the user fails to submit three dimensional Ground Control Points (GCPs). One has to purchase level 1A data (stereo pairs) of the required scene and some field survey is involved to generate such GCPs. These activities involve the cost and so limit the applicability of free DEMs.

Synergy of the Fusion:

DEM fusion has a synergistic effect based on the fundamental techniques by which optical stereoscopic and InSAR DEMs are produced and the reasons of failure of the individual techniques. We can predict complementarities in the error behavior of the stereoscopic and the InSAR techniques. The process of DEM generation with the optical stereoscopy fails, as stated above, in the presence of clouds or low texture, while the InSAR works fine in such cases. On the other hand, the InSAR fails under high terrain steepness or rapid change in surface roughness, both handled well with optical stereoscopy.

Problems of the InSAR technique like layover, temporal decorrelation or atmospheric effects may affect the phase of large areas in which the interferometric height determination fails leading to a regional error in DEMs. This phenomenon causes smoothing of DEM and thus introduces low frequency components in the frequency domain. In contrast to the InSAR case,

the stereo optical DEMs appear much more rugged and thus more difficult to interpret, as the detailed course of the terrain is hidden behind elevation spikes induced by conjugate point mismatches in the image pair. Therefore, the errors occur locally, typically as jumps between two adjacent pixels (Honikel 1998), which leads to high frequency components in the spatial frequency domain.

Previous Work:

DEM fusion approaches available in the literature can broadly be divided into two categories: fusion of DEMs from same source and fusion of DEMs from different sources. The later can be divided into two subclasses viz.; seamless and specific. Here, seamless means the methods designed to fuse DEMs irrespective of the sources and sensors; and specific means the methods designed for the particular sources or sensors.

Schultz et al. (1999) developed a methodology to fuse the stereoscopic DEMs. The methodology had two key steps: (1) detection of unreliable elevations estimates, and (2) fusion of the reliable elevations into a single optimal terrain model. In the stereoscopic technique, as the separation between the camera positions increases, elevation estimates become more precise (Kanade and Okutomi 1994). At the same time, widely separated viewpoints result in a substantial perspective distortion between images and increase the likelihood of encountering occlusions, which lead to false matches. The fusion took this tradeoff into consideration to model the terrain. They tested the effectiveness of the methodology, as well as the relationship between error rate and scene geometry by processing both real and photo-realistic simulations. The fusion process served several purposes, including improving the accuracy by averaging redundant elevation estimates, detecting and removing outliers, and estimating the geospatial uncertainty.

Slatton et al. (2002) combined the space-borne InSAR data from the ERS-1/2 platforms with multiple sets of airborne C-band InSAR data acquired by the NASA/JPL TOPSAR platform. They fused the InSAR data using a multi-scale Kalman smoothing approach. The estimated topography preserved the spatial resolution of the TOPSAR data while smoothing noise and providing estimates where there was no TOPSAR coverage.

Rao et al. (2003) used the optical stereo and the InSAR techniques to process the IRS-1C PAN stereo and ERS-1&2 tandem data respectively for DEM generation. They compared the products and carried out straightforward fusion by replacing the holes of one product with data from other product.

Honikel (1999) introduced a DEM fusion process, which took advantage of synergy between InSAR DEM and stereo-optical DEM generation, by weighting the height values in both DEMs according to the estimated error. He tested the approach with SPOT and ERS DEMs having very different accuracies. However, the terrain of the test area was again relatively flat (height difference 310 m).

Crosetto and Crippa (1998) proposed two level of integration. They first used the SPOT derived DEM to refine the interferometric flattening. Later they used prior knowledge in the implementation of ghost-line unwrapping technique (Goldstein et al. 1988) to locate ghost lines more precisely. Another level of fusion was performed in all of the available DEMs. They used weighted interpolation of SPOT DEM and InSAR DEMs from ascending and descending pairs to jointly estimate the terrain.

Honikel (1998) used the synergy between optical DEM and RADAR DEM in the spatial frequency domain. Mainly, the errors in the optical DEMs are prone to higher frequencies and than the RADAR DEMs which are prone to lower frequencies. In this work, the error prone

components of SPOT DEM and ERS-1 DEM where filtered out and the resulting spectra were combined in the frequency domain resulting to an improved DEM in terms of RMSE and error distribution.

Tannous and Goff (1996) presented a methodology for the fusion of image-based 3D information, such as interferometric ERS data, stereoscopic ERS data and stereoscopic SPOT data, for DEM generation. Their principle goal was to combine all the data in order to get the benefit of each of the available sensors so as to provide a DEM being more operational in terms of the density of reliable information and accuracy.

Very few studies have been reported in the literature in this field of data fusion. Moreover, almost all of them tested their algorithms for ERS 1 and ERS 2 tandem pair (as a SAR product) and SPOT (as an optical product). In addition, the work have been limited to relatively flat and low elevation areas of Europe and Indian plains. Results from these studies cannot directly be ported to the new dataset like ASTER, SRTM and ENVISAT and for the applications in rugged terrain.

The objective of this research was to assess the accuracy of DEMs generated by optical stereoscopy and InSAR and to develop a fusion technique to improve the overall accuracy. This paper introduces the approach developed to fuse the two freely available DEMs. The methodology addresses problems resulting from technological limitations of the optical stereoscopy and InSAR and exploits the good aspects of one product to minimize the shortcomings of another product.

Methodology:

The DEM fusion method developed in this research consisted primarily of pre-processing of DEMs and frequency domain fusion (Fig. 1). First, DEMs passed through the pre-processing steps of co-registration and void filling. Second, the Fast Fourier Transform (FFT) was applied to convert into frequency domain. Finally, typical low-pass and high-pass filters were applied to remove the erroneous frequency components from both of the DEMs before they were combined into a single DEM. In what follows, these steps of DEM fusion are briefly described.

Co-registration:

The relative ASTER DEM was co-registered to the SRTM DEM based on the GCPs collected over two DEMs. It is very difficult to select GCPs from DEMs because no distinct features like road crossings or river course are available that can be located precisely. To simplify this problem, valley lines and ridge lines were derived from the DEMs and crossing points of these geomorphic lines were carefully noted as GCPs. The co-registered ASTER DEM was then converted into near absolute DEM by shifting the histogram to the average elevation of the SRTM DEM.

Void Filling:

To fill the voids of one DEM, the slope and aspect of the void pixels were derived from elevations of the other DEM. These slope and aspect values, along with the absolute elevation of neighboring pixel were then used to determine the elevation of void pixels. This algorithm works only if there are data available in one of the participating DEMs where there is a hole in the other. The assumption is based on the synergy of errors between stereo-optical and InSAR techniques described above and is valid for practical purposes.

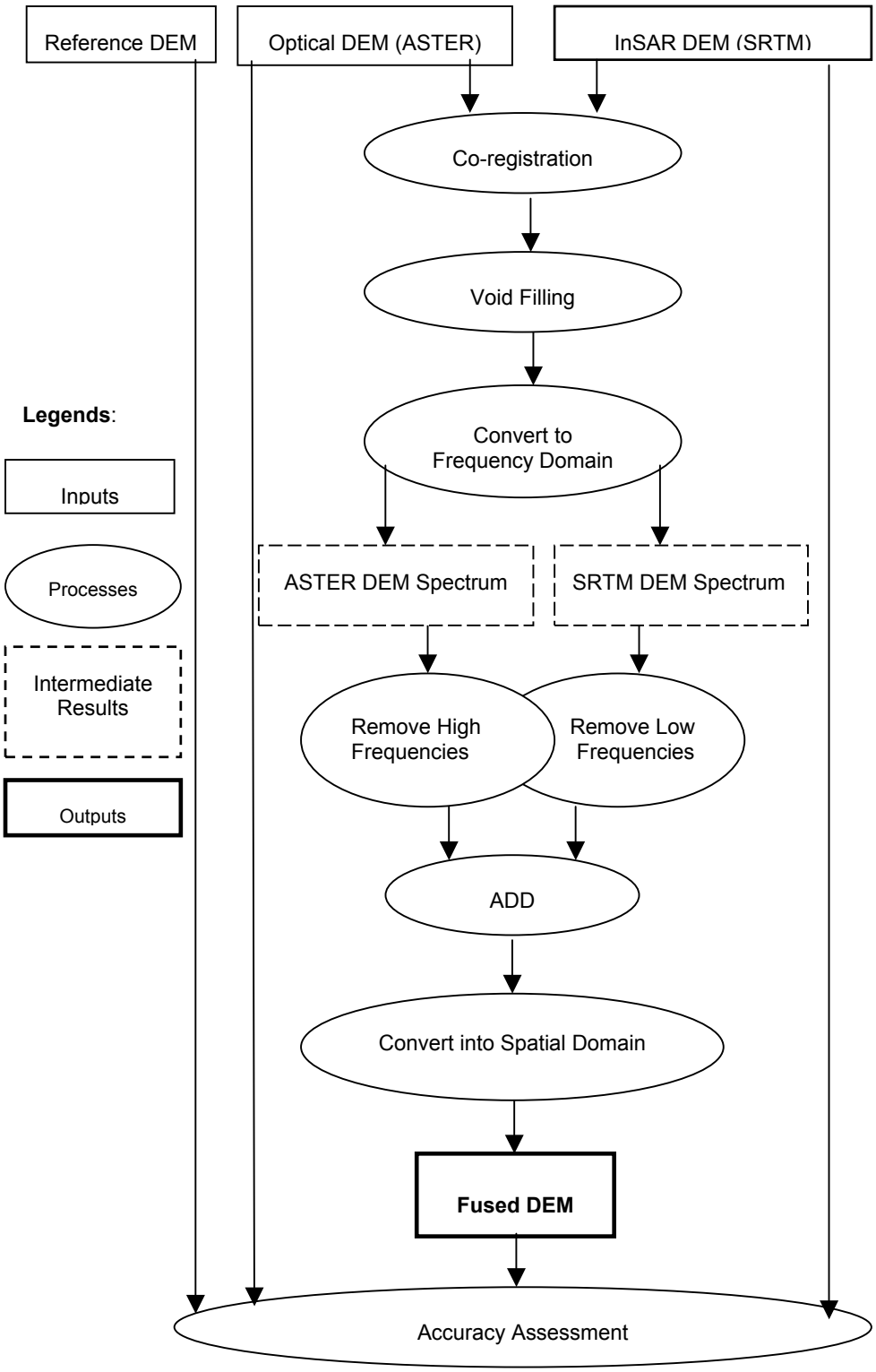

Fig 1: Flowchart of the Research. As shown in the legends, ovals are the processing blocks and rectangles are the data blocks

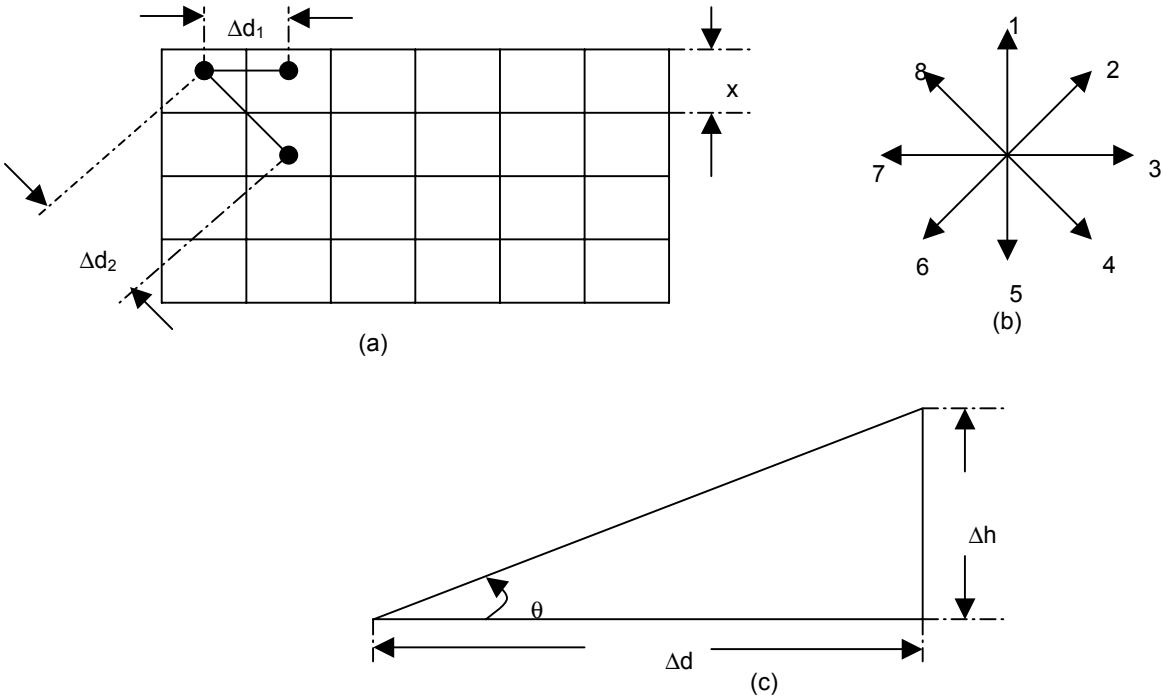

Fig. 2: Concept of Void Filling, (a) representation of pixel distance, (b) Aspect Representation, (c) Calculating elevation difference from slope map.

In the four-connectivity neighborhood of a digital image (Fig. 2.a), distance between two pixels is just the pixel size given by the equation (1). In the eight-connectivity, distance between diagonal pixels is given by the equation (2).

$\Delta d_1 = x$ (1)

$\Delta d_2 = x*\sqrt{2}$ (2)

where, Δd_1 and Δd_2 are the distances between two pixels in two different cases, and

x is the pixel size or resolution of the DEM.

Slope and aspect were classified into eight different classes (Fig. 2.b). If the classified aspect is odd, distance between two pixels in the direction of slope holds the equation (1). Otherwise, the equation (2) should be used.

Now, having calculated the distance between two pixels, the elevation difference between two pixels was calculated using the slope between the two pixels (Fig. 2.c). In this right angle triangle,

$\Delta h = \tan(\theta) * \Delta d$ (3)

where, Δh is the elevation difference between two pixels,

θ is the slope angle, and

Δd is the distance between two pixels (Eqns 1 and 2).

Elevation of a void pixel was then calculated as,

$h = elevation_{neighbor} \pm \Delta h$ (4)

where h is the elevation of void pixel and $elevation_{neighbor}$ is the elevation of the neighboring pixel. The positive sign before Δh was used when the neighboring pixel was at a lower elevation, and the negative sign was used when neighboring pixels were at a higher elevation.

The void filling strategy was then applied to DEMs in row by row fashion. When a void pixel was found in a row, an eight-connectivity search was used starting from the north direction to locate a consecutive neighbor pixel which was not a hole. The first pixel found was used to calculate the elevation of the hole pixel being treated. This search may fail in the case where there is a hole in the top-left corner of the image. Special treatment was applied to this case by allowing the search algorithm to go beyond the consecutive neighbors, and the hole pixels were filled recursively.

Frequency Domain Fusion:

First, the Fast Fourier Transform (FFT) was applied to each DEM to convert them into the spatial frequency domain. An ideal low pass filter was then implemented to remove the high frequency components from the ASTER DEM. The filtering operation was represented by the following equation (Honikel 1998).

$F_{lp}(p,q) = F(p,q)H_{lp}(p,q)$

where, p,q are the pixel locations in frequency domain,

$F_{lp}(p,q)$ is the resulting filtered DEM 2D spectrum.

F(p,q) is orginal Stereo Optical DEM 2D spectrum, and

$H_{lp}(p,q)$: Ideal low pass filter defined by the equation

$$H_{lp}(p,q) = \begin{cases} 1 & for \sqrt{(p^2+q^2)} < \varpi_0 \\ 0 & Otherwise \end{cases}$$

where, ϖ_0 is the cutoff frequency

A high pass filter with the same cutoff frequency (ϖ_0) was used to remove the low frequency components from the SRTM DEM. Determining good values of ϖ_0 may require some experiments to determine those best for a particular topography.Finally, the two spectrums were summed and inverse FFT converted the fused DEM back into spatial domain.

Test Site and Data:

The test site was located in central region of Nepal (85°32’ E, 27°36’N, 1530 m asl) some 25 km east of Kathmandu, the capital city of Nepal. The test site covered about 6000 ha terrain consisting of varying topography including plain valleys, very rugged hilly region (slopes up to 60 degree), and the elevation range of 655 m (Maximum-1840 m and Minimum-1185 m asl). The two DEMs used were obtained without cost. We had downloaded 3 arcsecond (~90m) SRTM InSAR DEM and ordered 30m ASTER relative DEM to cover the test site. The SRTM DEM was oversampled to 30m to make the datasets of equal resolution. Seasonal cultivation was the main landuse type in low land area whereas forest (mainly pine trees) was the main cover of upland region. Reference data for the study were purchased from the Survey Department of Nepal. This was a 1:25000 contour map developed by the Survey Department of Nepal in co-operation with the Finish International Development Agency (FNNIDA). This contour

map was interpolated to generate the reference DEM of 30m pixel size. UTM with Indian datum was the reference projection system. The test site falls in zone 45N.

Results:

The SRTM DEM of the test site looks coarse as originally the dataset was of ~90m resolution (Fig 3.a). The void in the central hill slope may be due to the geometry related constraints like shadows and foreshortening. The ASTER relative DEM had a void in the northwestern hilltop, which may be due to the cloud cover in the stereo images (Fig 3 .b).

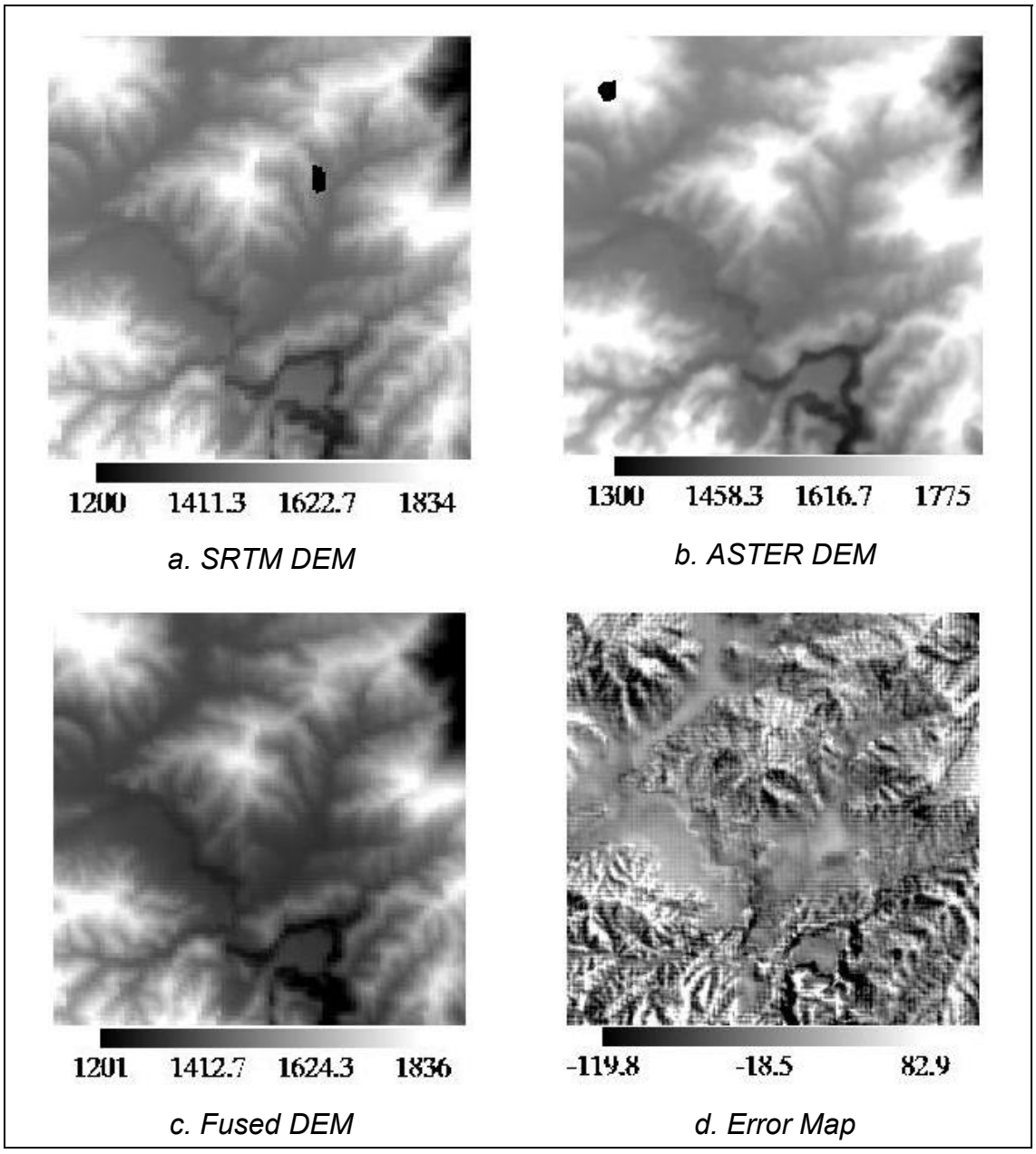

Fig. 3: The SRTM DEM with a void caused possibly by RADAR Geometry (a), The ASTER Relative DEM shifted to SRTM mean elevation having a void caused possibly by cloud cover (b), Fused DEM (c) and error map (d). All the scales used in the figure are in units of meters.

Error maps were computed by subtracting individual DEMs from the reference DEM and represented in signed magnitude form. So, the darker regions in the error maps (Fig. 3.d) represent the higher negative errors whereas the lighter regions represent the higher positive errors. The gray region in the map is the area with lowest absolute error.

The SRTM DEM had a higher average elevation, –8.7 m (Fig. 4, Table 1), than the reference DEM. The SRTM DEM had a negligible number of pixels with absolute errors greater than 100m and 2.4% pixels with absolute errors between 50 m to 100 m.

The ASTER DEM had been co-registered and shifted to the mean elevation of the SRTM DEM. So the error mean of this DEM was same as the error mean of the SRTM DEM. However, it was worse than the SRTM DEM in measures like standard deviation and range of the error. For the ASTER DEM, the standard deviation of the error was 28.3 m where for the SRTM DEM it was 18.3 m.

The fused DEM showed improvement in accuracy, completeness, and reliability. Though the mean error of the fused DEM was similar to the input DEMs, 44% improvement in the error standard deviation was observed with respect to the ASTER DEM. It was 12% better than the error standard deviation of the SRTM DEM. The peak errors (above 50m absolute) had been reduced to 2.3% from 7% for the ASTER and 2.4% for the SRTM. The error range of the

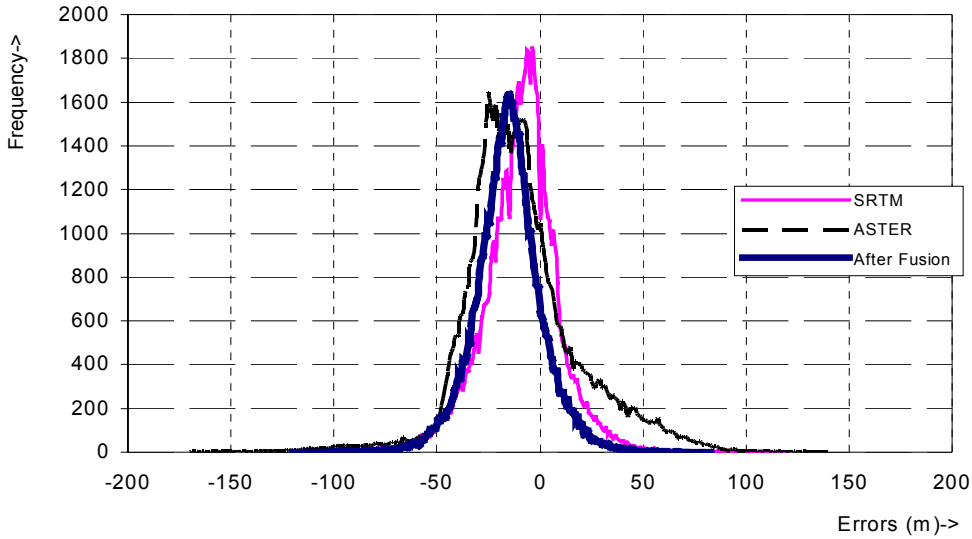

Fig 4: Histograms of Error Maps. Means of all the histograms are same. Improvement of the error statistics after fusion can be seen in the reduced standard deviation and reduced range of errors. The sharper shape of the error histogram after fusion depicts the fact.

resulting DEM was reduced to 201 m (Min: -119 m, Max: 82 m) from 308 (Min: -169 m, Max: 139 m) of the ASTER DEM and from 239 m (Min: -121 m, Max: 118 m) of the SRTM DEM. The fusion resulted to a DEM with a 30 m resolution preserving the resolution of the ASTER relative DEM.

Table 1. Key statistics measures of the DEM error histograms.

Error DEMs	Minimum (m)	Maximum (m)	Mean (m)	Standard Deviation (m)	Absolute Error >100 m	100 m>Absolute Error>50 m
SRTM	-121	118	-8.7	18.3	0.0%	2.4%
ASTER	-169	139	-8.7	28.3	0.6%	6.4%
Fused	-119	82	-8.7	16.4	0.0%	2.3%

The participating DEMs had holes covering about 1% of the test area. The fusion technique filled the holes and improved the completeness of the DEMs to 100%. These improvements over the accuracy and the completeness were vital to improve the reliability and thus the applicability of the products.

Conclusion:

The proposed methodology of data fusion benefited from the complementary error phenomena of the two DEMs and resulted to a significant improvement in the accuracy measures. From this research, we can conclude that,

- As compared to the ASTER relative DEM, the technique achieved up to 44% improvement in standard deviation and range of the error map while maintaining the resolution of 30 m. Similarly, as compared to the SRTM DEM, the technique improved the resolution to 30 m from 90 m while maintaining an accuracy level. It shows that the frequency domain fusion of the DEMs is an effective technique to improve the accuracy and consequently the reliability of satellite DEMs.
- The void filling technique filled all the voids. The topography filled by the approach was reasonably well fitted to the actual topography. So, the technique is very useful to increase the completeness and the applicability of the satellite DEMs to engineering applications.

The GCP based co-registration applied in this research has the accuracy of few pixels. In the future, image co-relation based co-registration will be implemented to achieve sub-pixel accuracy. The validity of the results is subject to the sufficient number of test applications. The proposed methodology will be evaluated for more test sites having different types of topography.

References:

Crosetto, M. and B. Crippa. 1998. Optical and RADAR data fusion for DEM generation. *IAPRS.* 32(4).

Ghiglia, D.C and M. D. Pritt. 1998. *Two-Dimensional Phase Unwrapping: Theory, Algorithms And Software*. New York, N.Y., USA: John Wiley & Sons.

Goldstein, R.M., H. Zebker, C. Werner. 1988. Satellite radar interferometry: two-dimensional phase unwrapping. *Radio Science.* 23(4): 713-720.

Graham, L.C. 1974. Synthetic Interferometer Radar for Topographic Mapping. *Proc. IEEE*, 62: 763-768.

Harold, R. and L. Roy. 1999. *Welch Algorithm Theoretical Basis Document for Aster Digital Elevation Models.* Athens, GA, USA: The University of Georgia.

Honikel, M. 1998. Fusion of Optical and Radar Digital Elevation Models in the Spatial Frequency Domain. *Retrieval of Bio- and Geo-Physical Parameters from SAR Data for Land Applications Workshop ESTEC.*

Honikel, M. 1999. Strategies and methods for the fusion of digital elevation models from optical and SAR data. *Proceedings of the Joint ISPRS/EARSeL Workshop "Fusion of Sensor Data,Knowledge Sources and Algorithms for Extraction and Classification of Topographic Objects".* 31(5):83-89

Kamp, U., T. Bolch and J. Olsenholler. 2003. DEM generation from ASTER satellite data for geomorphometric analysis of Cerro Sillajhuya, Chile/Bolivia. *ASPRS 2003 Annual Proceedings*.

Kanade, T. and M. Okutomi. 1994, A Stereo Matching Algorithm With an Adaptive Window: Theory and Experiment. *IEEE Trans. Pattern Analysis and Machine Intelligence*., 16(9): 920-932.

Koch, A., C. Heipke and P. Lohmann. 2002. Analysis of SRTM DTM: Methodology and Practical Results*. Geospatial Theory, Processing and Applications ISPRS Commission IV, Symposium*.

Rabus, B., M. Eineder, A. Rith and R. Bamler. 2003. The Shuttle Radar Topography Mission- A New Class of Digital Elevation models acquired by space borne radar. *ISPRS Journal of Photogrammetry and Remote Sensing.* 57: 241-262.

Rao, Y.S., K.S. Rao, G. Venkataraman, M. Khare and C. D. Reddy. 2003. Comparison and Fusion of DEMs Derived from InSAR and Optical Stereo Techniques. *Third ESA International Workshop on ERS SAR Interferometry*.

Schultz, H., E. M. Riseman, F. R. Stolle, and D.M. Woo. 1999. Error Detection and DEM Fusion Using Self-Consistency*, 7th IEEE International Conference on Computer Vision*.

Slatton, K. C., S. Teng, and M. Crawford. 2002. Multiscale Fusion of InSAR Data for Hydrological Applications. *Symposium on Terrain Analysis for Water Resources Applications*.

Tannous, I. and F. L. Goff. 1996. An integrated methodology for DEM computation through the fusion of interferometric, radargrammetric and photogrammetric data. *Fringe Workshop.*

Toutin, T., and L. Gray. 2002. State-of-the-art of elevation extraction from satellite SAR data. *ISPRS - Commission III Symposium*.

Zebker, H. and R. Goldstein. 1986. 'Topograhic Mapping from Interferometric Synthetic Apeture RADAR Observations. *Journal of Geophysical Research.* 91(B5): 4993-4999.

Zebker, H. and J. Villasenor. 1992. Decorrelation in Interferometric RADAR Echoes. *IEEE Transaction of Geoscience and Remote Sensing*. 30(5): 950-959.

Zebker, H.A., P.A. Rosen and S. Hensley. 1997. Atmospheric Effectgs in Interferometric Synthetic Aperture RADAR Surface Deformation and Topographic Maps. *Journal of Geophysical Research.* 102(B4): 7547-7563.